

A MEAN-FIELD THEORY FOR COARSENING FACETED SURFACES

SCOTT A. NORRIS AND STEPHEN J. WATSON

ABSTRACT. A mean-field theory is developed for the scale-invariant length distributions observed during the coarsening of one-dimensional faceted surfaces. This theory closely follows the LSW theory of Ostwald ripening in two-phase systems [1, 2, 3], but the mechanism of coarsening in faceted surfaces requires the addition of convolution terms recalling the work of Smoluchowski [4] and Schumann [5] on coalescence. The model is solved by the exponential distribution, but agreement with experiment is limited by the assumption that neighboring facet lengths are uncorrelated. However, the method concisely describes the essential processes operating in the scaling state, illuminates a clear path for future refinement, and offers a framework for the investigation of faceted surfaces evolving under arbitrary dynamics.

1. INTRODUCTION

In many examples of faceted surface evolution, a *facet velocity law* giving the normal velocity of each facet can be observed, assumed, or derived. Examples of such dynamic laws describe growth of polycrystalline diamond films from the vapor [6, 7], evolution of faceted boundaries between two elastic solids [8], the evaporation/condensation mechanism of thermal annealing [9], and various solidification systems [10, 11, 12, 13, 14]. Such velocity laws are typically configurational, depending on surface properties of the facet such as area, perimeter, orientation, or position, and reduce the computational complexity of evolving a continuous surface to the level of a finite-dimensional system of ordinary differential equations. This theoretical simplification enables and invites large numerical simulations for the study of statistical behavior. This has been done frequently for one-dimensional surfaces [10, 11, 12, 13, 14, 15, 16, 17, 18, 19], while less frequently for two-dimensional surfaces due to the necessity of handling complicated topological events [9, 20, 21, 22, 23, 24]. Such inquiries reveal that many of the systems listed above exhibit coarsening – the continual vanishing of small facets and the increase in the average length of those that remain. Notably, these systems also display *dynamic scaling*, in which common geometric surface properties approach a constant statistical state, which is preserved even as the length scale increases.

The dynamical scaling behavior of coarsening faceted surfaces recalls the process of Ostwald ripening [25], in which small solid-phase grains in a liquid matrix dissolve, while larger grains accrete the resulting solute and grow. As this proceeds, the distribution of relative particle sizes tends to a constant state¹. In fact, general 2D faceted surfaces fall conceptually into the same class of *phase-ordering*

Date: April 5, 2006.

¹Indeed, it was observed some time ago that facets of alternating orientations on a one-dimensional surface are analogous to alternating phases of a separating two-phase alloy [26, 27],

systems, except that the a vector order parameter reflecting surface normal replaces the scalar order parameter reflecting phase [31]; other systems exhibiting similar behavior include coarsening cellular networks describing soap froths and polycrystalline films [32, 33, 34, 35, 36], and films growing via spiral defect [37]. Each of these generalizations is characterized by a network of evolving boundaries which separate domains of possibly differing composition, and exhibit coarsening and convergence toward scale-invariant steady states.

Since dynamic scaling pushes complex systems into a state which can be effectively characterized by just a few statistics, it is natural to seek simplified models which replicate this behavior. The canonical example of this approach is the celebrated theory of Lifshitz, Slyozov, and Wagner describing Ostwald ripening [1, 2, 3]. Generically, such an approach selects a distribution of some quantity, and includes just enough of the total system behavior to specify the effective behavior of that quantity – for example, the original LSW theory first identifies the average behavior of particles as a function of size, and uses that result to identify a continuity equation describing distribution evolution. Ideas of this kind have been applied to several of the higher-order cellular systems introduced above – for soap froths [38, 39], polycrystals [], and spiral-growth films [37]. To the extent that such approaches mirror experimental data, they can yield valuable physical insight which cannot be gained by considering single particles, nor even by direct numerical simulation of larger ensembles. However, to date no similar attempt has been made for evolving faceted interfaces.

Given the wide variety of examples of purely faceted motion, the membership of this problem class in the wider class of phase ordering systems, and the past success in applying mean-field analyses to these systems, it is somewhat surprising that no such attempt has been made to describe the mean-field evolution of faceted surfaces. In this chapter, therefore, we take a first step in that direction by introducing a framework for describing the distribution of facet lengths in 1D faceted surface evolution. Our approach closely resembles the LSW theory of Ostwald ripening, in that a facet-velocity law allows the effective behavior of facets by length, and thus the specification of a continuity equation governing the evolution of the length distribution. However, our model differs in that facets do not vanish in isolation as do grains in Ostwald ripening – instead each vanishing facet causes its two immediate neighbors to join together. This process of merging is not treated in LSW theory, and requires the introduction of a convolution integral reminiscent of equations due to Smoluchowski [4] and Schumann [5] describing coagulation. We apply our method to one particular facet dynamics, associated with the directional solidification of faceting binary alloys. However, the method is general and can be applied to any dynamics where effective facet behavior is accessible.

2. EXAMPLE DYNAMICS AND PROBLEM FORMULATION

During the directional solidification of a strongly anisotropic binary alloy, small-wavelength faceted surfaces develop. If the alloy is solidified above a critical velocity, a layer of supercooled liquid is created at the interface, which drives a coarsening

and the Cahn-Hilliard equation [28] which models phase separation has been used, in modified form, to describe several different kinds of faceted surface evolution [29, 30, 14].

instability governed by the facet dynamics [14]

$$(1) \quad \frac{dh_i}{dt} = \langle h_i \rangle.$$

Figure 1a displays representative surface evolution during coarsening. There, the locations of corners are plotted over time. We see that this system exhibits *binary coarsening*, whereby a single facet shrinks to zero length, causing two corners meet and annihilate. As coarsening proceeds, the average facet length increases (Figure 1b), and a scale-invariant distribution of relative facet lengths is reached (Figure 1c).

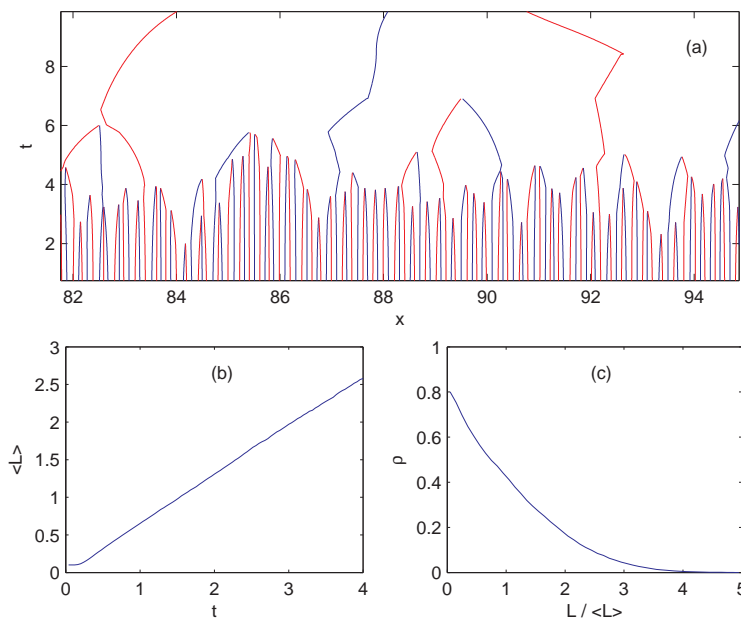


FIGURE 1. Survey of coarsening behavior. (a) A representative example of the kink/anti-kink evolution (red/blue). (b) Facet lengthscale growth with time. (c) Scale-invariant distribution of relative facet lengths (the tail is gaussian).

To describe the evolution of a scale-invariant length distribution such as that shown in Figure 1c, we will think in terms of a mass-transport problem. We will derive equations governing the evolution of the mass distribution $P(x)$, where mass “particles” at position x correspond to facets with length $L = x$. Here $P(x)$ is not necessarily a probability distribution, and so its mass is not assumed to be unity. Thus, it will be useful to also consider the unit-mass scaling of this function, $\hat{P}(x) = P(x) \div \int_0^\infty P(x)dx$, which is a true probability distribution. The goal, of course, is to model \hat{P} , but we will begin with a simple equation governing the evolution of P , and add terms until that equation governs both P and \hat{P} . To simplify the calculations, we will assume that (a) all facets have slopes of ± 1 , (b) facets vanish via binary coarsening, (c) neighboring facet lengths are uncorrelated. Additionally, in what follows, it will be helpful to consider Figure 2, which shows a representative facet F , and its two neighbors $F^{(-)}$ and $F^{(+)}$.

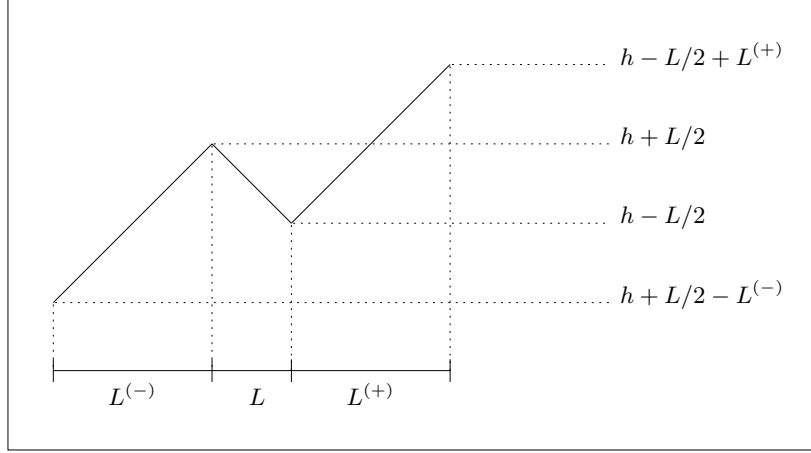


FIGURE 2. A diagram illustrating a representative facet and its two neighbors. Here h is an arbitrary reference height that occurs at the midpoint of the center facet.

2.1. Flux Law. We begin by observing that, because all slopes are fixed with alternating values ± 1 , then the rate of length change for any single facet is independent of its own vertical velocity, and is instead completely determined by the vertical velocity of its immediate neighbors. This general, geometric property can be obtained by inspection of Figure 2, and may be written

$$(2) \quad \frac{dL_i}{dt} = \frac{1}{2}(-1)^i \left[\frac{dh_{i+1}}{dt} - \frac{dh_{i-1}}{dt} \right].$$

where odd (even) facets have negative (positive) slopes. Assume for now that a consideration of the facet dynamics (1), the existing distribution P , and Equation (2) allow the derivation of an effective mean facet behavior

$$(3) \quad \phi(L) = \left\langle \frac{dL}{dt} \right\rangle (L),$$

which gives the average rate of length change as a function of facet length. Then we can use the divergence theorem to write a simple continuity equation for P , letting x take the place of L :

$$(4) \quad \frac{\partial P}{\partial t} + \frac{\partial}{\partial x} [P(x)\phi(x)] = 0,$$

where $\phi(x)$ now represents the effective lateral velocity of particles at position x , and $P\phi$ then gives the total mass flux.

2.2. Accuracy: describing coarsening. Since equation (4) aims to describe a coarsening problem, it must accurately address the primary feature of coarsening – the shrinking and vanishing of facets over time. To see if it does, we consider Figure 2 again, and imagine that the facet F goes to length 0. We see that three things occur: first, the facet F itself vanishes; second, the neighbors of F also vanish; and third, a new facet is created which is the merging of the neighbors of

F . If these processes are not captured by Eqn. (4), then we must add terms to it so that it does.

The first process of facet vanishing is indeed captured by the flux equation (4). In the mass-transport framework, vanishing facets are represented by mass particles of $P(x)$ flowing out of the domain through the boundary at $x = 0$. Equation (4) naturally exhibits this behavior, and allows the easy extraction of the relative rate R at which coarsening occurs. This is simply the flux at the origin, given by

$$(5) \quad R = -P(0)\phi(0).$$

The second process, neighbor loss, is not captured by (4). To include it, we model it as a *mass sink* S , which must subtract mass in a way that is probabilistically accurate. Recalling the assumption that adjacent facet lengths are not correlated, we can assume that L_{i-1} and L_{i+1} are each described by the (probability) distribution $\hat{P}(x)$. Thus, the appropriate sink is

$$(6) \quad S(x) = -2\hat{P}(x).$$

The final process of facet creation is also not captured by (4). We model it, in contrast to neighbor loss, as a *mass source* Ψ , which produces facets of length $L_{i-1} + L_{i+1}$. Since these variables are independent, and each described by P , then the sum $L_{i-1} + L_{i+1}$ is described by the joint probability function

$$(7) \quad \Psi(x) = \hat{P}_2(x) = \int_0^x \hat{P}(s)\hat{P}(x-s) ds,$$

obtained by integrating a two-point (probability) distribution $\hat{P}(x)\hat{P}(y)$ along lines of constant $x + y$.

The net modifications required by coarsening may now be summed into a single term

$$(8) \quad C(x) \equiv S(x) + \Psi(x) = -2\hat{P}(x) + \int_0^x \hat{P}(s)\hat{P}(x-s) ds.$$

Since C describes the additional effects of particles leaving the domain (i.e. coarsening), it must be multiplied by R , the rate at which this occurs, and then added to Eqn. (4). This gives the result

$$(9) \quad \frac{\partial P}{\partial t} = -\frac{\partial}{\partial x}(\phi P) + \mathcal{R}C(x).$$

2.3. Convenience: preserve mass and center of mass. Equation (9), with C defined as in (8), now correctly describes the mass redistribution associated with coarsening. In particular, it models the two primary features of coarsening – the decrease in the number N of facets over time, and the corresponding increase in the average length L of those that remain. In the language of a mass-transport equation, these correspond respectively to a decrease in the total mass, or zeroeth moment $\mathcal{M}^{(0)}$, and an increase in the center of mass, or first moment $\mathcal{M}^{(1)}$, given respectively by

$$(10a) \quad \mathcal{M}^{(0)} = \int_0^\infty P(x)dx$$

$$(10b) \quad \mathcal{M}^{(1)} = \frac{1}{\mathcal{M}^{(0)}} \int_0^\infty xP(x)dx.$$

Indeed, by performing the above integrations against the whole of Eqn. (9) (rather than just against P), we can establish that

$$(11a) \quad \frac{\partial \mathcal{M}^{(0)}}{\partial t} = -2\mathcal{R}$$

$$(11b) \quad \frac{\partial \mathcal{M}^{(1)}}{\partial t} = \int_0^\infty \phi \hat{P} dx.$$

These rates of change in $\mathcal{M}^{(0)}$ and $\mathcal{M}^{(1)}$ are an accurate description of the relative change in the number of facets and average length scale of any initial faceted surface. However, the aim of this work is to obtain a description of the steady, dynamically scaling distribution of relative facet lengths. This function has not only fixed unit mass as \hat{P} , but also a fixed unit moment. Thus, in this step we perform a dynamic non-dimensionalization to ensure that both quantities are naturally kept constant.

To keep $\mathcal{M}^{(0)}$ constant, or functionally to make P identically \hat{P} , we observe in Figure 2 that, for each coarsening event, two facets are lost in total. Thus, if the rate of coarsening events is R , the net relative rate of mass loss is $2R$ – indeed, this agrees with Eqn. (11a). To keep total mass neutral, we must add mass back into the system at the same rate, in a way that is probabilistically accurate. What we want to do conceptually is to simply increase the weight of each particle that remains in the system, thus preserving total mass without moving any particles. This is accomplished mathematically by adding mass particles in precisely the proportion that they already exist, as represented by a re-weighting term

$$(12) \quad W(x) = 2\hat{P}(x).$$

Finally, to keep $\mathcal{M}^{(1)}$ constant, we non-dimensionalize the problem with the *time-dependent* lengthscale $L(t)$ as follows:

$$(13) \quad \bar{x} = \frac{x}{L(t)}, \quad \bar{\phi} = \frac{\phi}{L(t)}, \quad \bar{P} = L(t)P, \quad \bar{C} = L(t)C.$$

Since the average lengthscale in the system is constantly increasing due to coarsening, the scaling for x compresses P laterally to keep the center of mass at unity. However, to make sure that mass (area) is not also reduced, we also perform the scaling shown on P which stretches P vertically, preserving total area, and thus, mass. The unknowns ϕ and C are formally scaled as well; ϕ is a velocity, and so receives the same scaling as x , while C is the sum of two distributions, and so receives the same scaling as P .

Making this substitution and properly applying the chain rule² results in a final, scale-invariant description of the evolution of the relative length distribution (note

² In particular, application of these scalings to the term $\partial P / \partial t$ yields

$$\frac{\partial P}{\partial t} \rightarrow \frac{1}{L} \left[\frac{\partial \bar{P}}{\partial t} - \frac{1}{L} \frac{dL}{dt} \left(\bar{x} \frac{\partial \bar{P}}{\partial \bar{x}} + \bar{P} \right) \right]$$

which contains the term $(L^{-1})dL/dt$. This is undesirable, as we don't want to keep track of L explicitly. However, $L \sim N^{-1}$, and so $(L^{-1})dL/dt = -(N^{-1})dN/dt$, which is a relative rate of facet loss. However, we have already defined a similar quantity. Since R describes the relative rate of particle loss through the origin, and since two facets vanish for each lost particle (consider Figure 2),

$$\frac{1}{L} \frac{dL}{dt} = -\frac{1}{N} \frac{dN}{dt} = 2R.$$

that S and W cancel)

$$(14) \quad \frac{\partial P}{\partial t} = -\frac{\partial}{\partial x}[P(x)\phi(x)] + \mathcal{R} \left[P_2(x) + 2\left(P + x\frac{\partial P}{\partial x}\right) \right];$$

note that while P was not assumed to necessarily preserve mass nor moment, it has been manipulated to do so, and is thus a true probability function. This result is quite general, and describes the evolution of the lengthscale distribution for any facet dynamics which admits an effective particle velocity ϕ . Generally, we see that there is a competition between the P_2 term, which redistributes mass toward infinity, and the $(\partial/\partial x)(xP)$ term, which pushes mass toward zero. This competition is then modulated by the appropriate dynamics ϕ .

3. APPLICATION: OUR CHOSEN FACET DYNAMICS

The framework just derived was completely general, describing the coarsening of any faceted surface, and indeed any binary system exhibiting binary coarsening. We here apply that general framework to the specific facet dynamics (1), by deriving the appropriate effective flux function $\phi(x)$. Using the dynamics itself, the general kinematic form of ϕ given in Equation (2), and recalling the diagram in Figure 2, we perform the following calculation:

$$(15a) \quad \frac{dL}{dt} = \frac{1}{2} \left(\frac{dh^{(-)}}{dt} - \frac{dh^{(+)}}{dt} \right)$$

$$(15b) \quad = \frac{1}{2} \left(\langle h^{(-)} \rangle - \langle h^{(+)} \rangle \right)$$

$$(15c) \quad = \frac{1}{2} \left(\frac{1}{2}[2h + L - L^{(-)}] - \frac{1}{2}[2h - L + L^{(+)}] \right)$$

$$(15d) \quad = \frac{1}{2} \left(L - \frac{1}{2}[L^{(-)} + L^{(+)}] \right)$$

$$(15e) \quad = \frac{1}{2} \left(L - \frac{1}{2} \int_0^\infty x P_2(x) dx \right)$$

$$(15f) \quad \phi(x) = \frac{1}{2} (x - L(t))$$

$$(15g) \quad \bar{\phi}(\bar{x}) = \frac{1}{2} (\bar{x} - 1).$$

In step (15e), since both $L^{(-)}$ and $L^{(+)}$ obey the distribution P , the sum $L^{(-)}$ and $L^{(+)}$ is again modelled by the joint probability function P_2 . The effective contribution to ϕ is then obtained by performing a weighted integral of possible sums x multiplied by their relative prevalence P_2 . Since the total mass of P_2 equals unity, that integration describes the center of mass of P_2 , which by considering the form of Eqn. (7) can be shown to equal $2\mathcal{M}^{(1)} = 2L(t)$. This result, in turn, informs the final nondimensionalized result in step (15g).

Having calculated ϕ , we now write the complete evolution equation for the distribution of relative facet lengths under the specific facet dynamics (1):

$$(16) \quad \frac{\partial P}{\partial t} = -\frac{1}{2} \frac{\partial}{\partial x}[(x-1)P] + R \left[\int_0^x P(s)P(x-s) ds + 2\frac{\partial}{\partial x}(xP(x)) \right].$$

Remark. We see that the flux (15g) is negative for facets smaller than the average, and positive for facets larger than the average. Broadly speaking, this is

how coarsening works – small facets shrink and vanish, while large facets grow at their expense. Thus, our approximation at least has the right form.

4. SOLUTION AND COMPARISON WITH NUMERICAL-EXPERIMENTAL DATA

Solution of Equation (16) is currently performed numerically, by letting arbitrary initial conditions relax to a steady state; our numerical method is given in Appendix A. This state is unsurprisingly independent of the initial condition chosen, but surprisingly simple in form – it is simply the exponential distribution $P(x) = \exp(-x)$, which is easily shown (after the fact) to satisfy Equation (16). We now proceed to compare the characteristics of this predicted steady state with those of the actual steady state found by direct simulation of the dynamics (1); our main results are shown in Figure 3.

We begin in Figure 3a by comparing the distribution P itself. The predicted exponential distribution is shown in blue; comparison with the green actual distribution reveals qualitative but not quantitative agreement. In particular, while the tail of the predicted distribution is (obviously) exponential, the tail of the actual distribution is gaussian. As a consequence, our mean-field steady state exhibits far too great an incidence of extremely long facets.

Seeking the cause of this discrepancy, we next test the accuracy of our effective flux function $\phi(x)$. Figure 3b shows the contour plot of the distribution of length/velocity pairs $\rho(x, \phi)$. Finding the mean velocity for each length gives the statistical ϕ (dashes), which turns out to compare favorably with the predicted ϕ (solid). Both are linear with form $\phi = \alpha(x - 1)$, and while the actual slope of 0.39 differs from the predicted slope of 0.5, they can be made to agree by simply scaling time, since every term in Equation (16) contains either ϕ or $\phi(0)$. So this approximation seems to be valid.

Finally, we examine the coarsening terms: the sink $S(x)$ in Figure 3c and the source $\Psi(x)$ in Figure 3d. These are functionals of P , and so we are not surprised that the predicted values (blue) are different from the values calculated from the actual steady state (green). However, for both S and Ψ , we assumed that neighboring facet lengths were uncorrelated. If we instead calculate statistically the S and Ψ generated by vanishing facets (that is, the *neighbors* of vanishing facets), we get the curves in red, which are different not only from the predicted quantities, but also from the quantities we would have gotten from using the actual distribution P and assuming no correlations.

This suggests that the ultimate culprit is the assumption that neighboring facet lengths are uncorrelated. Going back to the simulation, we now measure the correlation of the lengths of nearby facets as a function of neighbor distance, in Figure 4. There we see a small but significant correlation for at least the first two neighbors. This produces the discrepancy between the green and red curves in Figures 3c,d above, and may be responsible for the discrepancy in the tail as well. This result is not surprising, as the main weakness of the original LSW theory which inspires this work was also a failure to address correlations; later generalizations which corrected this deficiency agreed well with experimental data [40].

5. CONCLUSIONS

We have presented a mean-field theory for the evolution of length distributions associated with coarsening faceted surfaces. In the spirit of LSW theory,

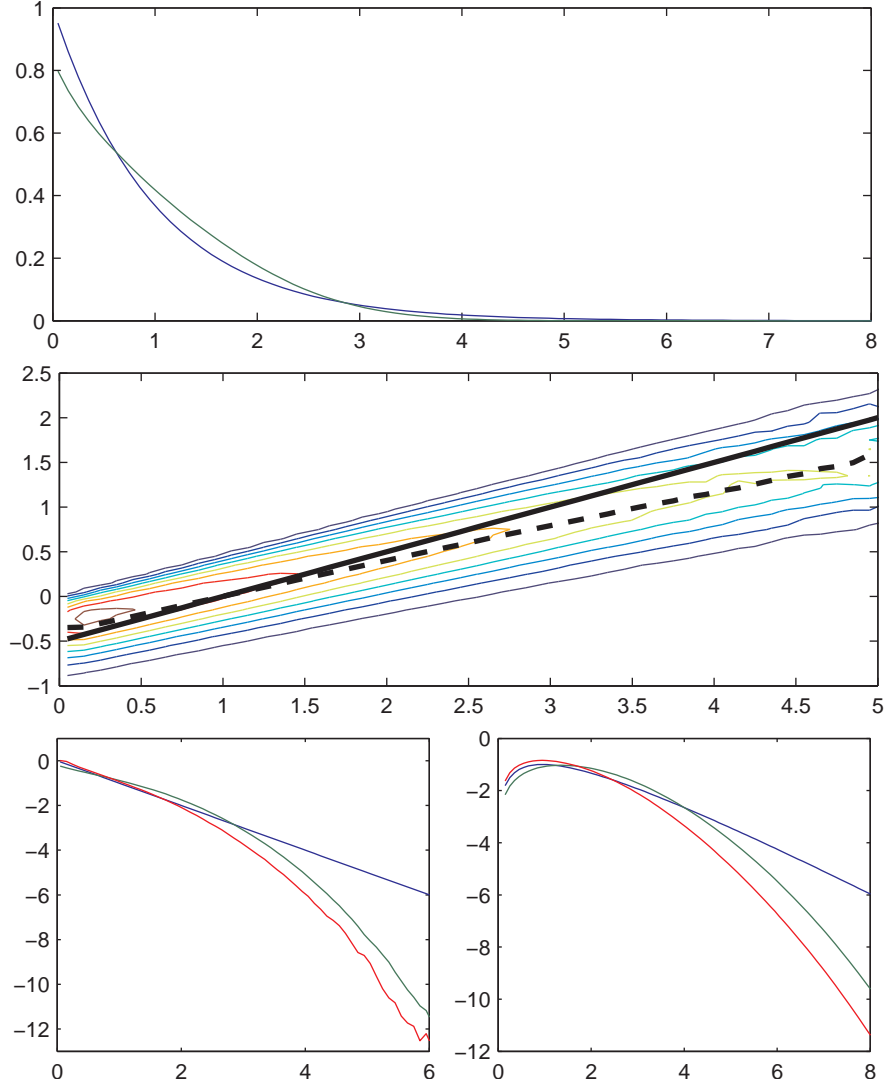


FIGURE 3. (a) Comparison between the theoretically-predicted (blue) and statistically-gathered (green) steady states. The former exhibits exponential decay, while the latter is gaussian. (b) Contour of the statistical distribution of length/velocity pairs $\rho(x, \phi)$. For each length, mean statistical velocity is plotted as dotted line, while the predicted velocity $\phi(x)$ is a solid line. (c,d) Comparison of $\log(-S/2)$, $\log(\Psi)$ as obtained by various means: from the predicted steady state (blue), from the actual steady state (green), and from measuring the neighbors of vanishing facets in the actual steady state (red).

a facet-velocity law governing surface evolution is used to establish a characteristic length-change law; this in turn leads to a simple continuity equation governing the

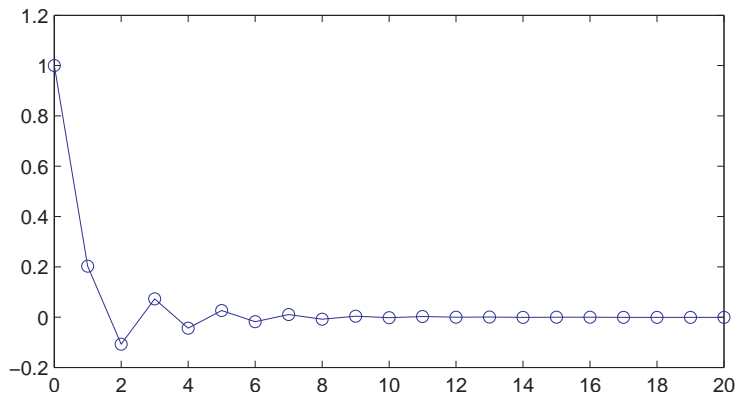


FIGURE 4. Statistically-sampled correlation of facet lengths as a function of neighbor distance.

evolution of the probability distribution. However, because the vanishing of any facet forces the joining of its two neighbors, this equation must be modified by the addition of appropriate terms describing coarsening, including a convolution term recalling models of coagulation. Our model therefore serves, apart from the direct application to facet dynamics, as a study in the union of these two mechanisms of steady statistical behavior.

The scale-invariant distribution is tracked by introducing an appropriate time-dependent non-dimensionalization, and the resulting equation is solved by the exponential distribution; numerical simulation reveals that any initial condition converges to this solution. This result unfortunately does not agree quantitatively with the more gaussian distribution obtained by sampling a large surface simulated directly under the facet dynamics. Further investigation reveals that the likely culprit is the assumption that neighboring facet lengths are uncorrelated. Indeed, a similar assumption plagued the original LSW theory, and relaxing that assumption resulted in much better agreement with experiment.

However, even with this deficiency, the model captures the essential feature of the dynamically scaling state – a particular mass flux law which drives coarsening by pushing mass away from unity, moderated by competing terms describing coarsening and continuous rescaling, which push mass toward infinity and zero, respectively. While later improvements to our model addressing neighbor correlation will undoubtedly increase its predictive capabilities, these same forces will still balance in the steady state. The model as presented thus serves as a qualitative explanation of the essential features of the scaling state, as well as a guide to further research efforts.

Acknowledgements. SAN was supported by NASA GSRP #NGT5-50434.

APPENDIX A. NUMERICAL SIMULATION

This section describes the simulation of Equation (16), which is repeated here for convenience:

$$\frac{\partial P}{\partial t} = -\frac{1}{2} \frac{\partial}{\partial x} [(x-1)P] + R \left[\int_0^x P(s)P(x-s) ds + 2 \frac{\partial}{\partial x} (xP(x)) \right].$$

Since the spatial derivatives here are purely advective, we use an upwinding finite difference scheme to approximate them, which easily captures the evolution of discontinuous initial conditions, and is accurate to second order in space. Standard Simpson's quadrature methods are used for the convolution integral. For time-stepping, a Crank-Nicholson integration on the linear terms combined with a second-order Adams-Bashforth integration of the integral is quite stable, allowing the use of large timesteps to quickly reach the relaxed steady state. However, two numerical issues arise that require special mention.

First, we note that the correct boundary condition on Eqn. (16) is that P vanishes at infinity. To be able to specify this condition, and also to include the whole domain using a finite number of grid points, we perform the change of variables $\xi = \exp(-x)$, which maps the domain $[0, \infty)$ to $[1, 0]$. The resulting equation, with like terms collected, is:

$$(17) \quad \frac{\partial P}{\partial t} = [(2\mathcal{R} - 0.5) \ln(x) - 0.5]x \frac{\partial P}{\partial \xi} + (2\mathcal{R} - 0.5)P + \mathcal{R} \int_{\xi}^1 \frac{1}{s} P(s)P(\xi/s) ds.$$

Now the entire domain of P is included, and the boundary condition at ∞ can be easily implemented; additionally, gridpoints are distributed unevenly, with a bias toward zero to increase resolution of the tail of P . Note, however, that the convolution describing P_2 now contains an integrable singularity requiring custom quadrature, and additionally requires an interpolation of P to obtain its values at the points ξ/s .

Second, while Eqn. (14) was reached by carefully including terms to conserve the mass $\mathcal{M}^{(0)}$ and center of mass $\mathcal{M}^{(1)}$, it turns out that neither is a numerically stable quantity. In fact, by performing appropriate multiplications and integrations, we can write down a system of ODEs governing the evolution of $\mathcal{M}^{(0)}$ and $\mathcal{M}^{(1)}$:

$$(18a) \quad \frac{\partial \mathcal{M}^{(0)}}{\partial t} = P(0) (\mathcal{M}^{(0)^2} - 1)$$

$$(18b) \quad \frac{\partial \mathcal{M}^{(1)}}{\partial t} = \mathcal{M}^{(1)}/\mathcal{M}^{(0)} - 1$$

From this dynamical systems perspective, the point $(\mathcal{M}^{(0)}, \mathcal{M}^{(1)}) = (1, 1)$ is indeed a fixed point, but an unstable one. This poses no problems for the theory per se, as equation (14) contains no mechanism for perturbing the solution away from this fixed point. However, inevitable numerical error will so perturb any calculation, after which such perturbation grows. To avoid this pitfall, it is thus necessary to periodically re-scale the solution manually back to this fixed point by interpolation.

REFERENCES

- [1] I. Lifshitz, V. Slezov, Kinetics of diffusive decomposition of supersaturated solid solutions, Soviet Physics JETP 38 (1959) 331–339.
- [2] I. Lifshitz, V. Slyozov, The kinetics of precipitation from supersaturated solid solutions, J. Phys. Chem. Solids 19 (1961) 35–50.

- [3] C. Wagner, Theorie der alterung von niederschlägen durch umlösen, *Zeitschrift für Elektrochemie* 65 (1961) 581–591.
- [4] M. von Smoluchowski, Drei vorträge über diffusion, brownsche molekularebewegung und koagulation von kolloidteilchen, *Physikalische Zeitschrift* 17 (1916) 557–571.
- [5] T. Schumann, Theoretical aspects of the size distribution of fog particles, *Quarterly Journal of the Royal Meteorological Society* 66 (1940) 195–207.
- [6] A. Kolmogorov, To the "geometric selection" of crystals, *Dokl. Acad. Nauk. USSR* 65 (1940) 681–684.
- [7] A. van der Drift, Evolutionary selection, a principle governing growth orientation in vapor-deposited layers, *Philips Research Reports* 22 (1967) 267–288.
- [8] M. Gurtin, P. Voorhees, On the effects of elastic stress on the motion of fully faceted interfaces, *Acta Materialia* 46 (6) (1998) 2103–2112.
- [9] S. Watson, S. Norris, Scaling theory and morphometrics for a coarsening multiscale surface, via a principle of maximal dissipation, *Physical Review Letters* 96 (2006) 176103.
- [10] L. Pfeiffer, S. Paine, G. Gilmer, W. van Saarloos, K. West, Pattern formation resulting from faceted growth in zone-melted thin films, *Physical Review Letters* 54 (17) (1985) 1944–1947.
- [11] D. Shangguan, J. Hunt, Dynamical study of the pattern formation of faceted cellular array growth, *Journal of Crystal Growth* 96 (1989) 856–870.
- [12] C. Emmot, A. Bray, Coarsening dynamics of a one-dimensional driven Cahn-Hilliard system, *Physical Review E* 54 (5) (1996) 4568–4575.
- [13] S. Watson, F. Otto, B. Rubinstein, S. Davis, Coarsening dynamics of the convective Cahn-Hilliard equation, *Physica D* 178 (3-4) (2003) 127–148.
- [14] S. Norris, S. Davis, P. Voorhees, S. Watson, Faceted interfaces in directional solidification, *Journal of Crystal Growth* 310 (2008) 414–427.
- [15] C. Wild, N. Herres, P. Koidl, Texture formation in polycrystalline diamond films, *Journal of Applied Physics* 68 (3) (1990) 973–978.
- [16] J. Thijssen, H. Knops, A. Dammers, Dynamic scaling in polycrystalline growth, *Physical Review B* 45 (15) (1992) 8650–8656.
- [17] Paritosh, D. Srolovitz, C. Battaile, J. Butler, Simulation of faceted film growth in two dimensions: Microstructure, morphology, and texture, *Acta Materialia* 47 (7) (1999) 2269–2281.
- [18] J. Zhang, J. Adams, FACET: a novel model of simulation and visualization of polycrystalline thin film growth, *Modeling Simul. Mater. Sci. Eng* 10 (2002) 381–401.
- [19] J. Zhang, J. Adams, Modeling and visualization of polycrystalline thin film growth, *Computational Materials Science* 31 (3-4) (2004) 317–328.
- [20] J. Thijssen, Simulations of polycrystalline growth in 2+1 dimensions, *Physical Review B* 51 (3) (1995) 1985–1988.
- [21] S. Barrat, P. Pigeat, E. Bauer-Grosse, Three-dimensional simulation of CVD diamond film growth, *Diamond and Related Materials* 5 (1996) 276–280.
- [22] G. Russo, P. Smereka, A level-set method for the evolution of faceted crystals, *SIAM Journal of Scientific Computing* 21 (6) (2000) 2073–2095.
- [23] P. Smereka, X. Li, G. Russo, D. Srolovitz, Simulation of faceted film growth in three dimensions: Microstructure, morphology, and texture, *Acta Materialia* 53 (2005) 1191–1204.
- [24] S. Norris, S. Watson, Geometric simulation and surface statistics of coarsening faceted surfaces, *Acta Materialia* 55 (2007) 6444–6452.
- [25] W. Ostwald, *Z. Phys. Chem.* 34 (1900) 495.
- [26] W. Mullins, Theory of linear facet growth during thermal etching, *Philosophical Magazine* 6 (71) (1961) 1313–1341.
- [27] N. Cabrera, On stability of structure of crystal surfaces, in: *Symposium on Properties of Surfaces*, ASTM Materials Science Series – 4, American Society for Testing and Materials, American Society for Testing and Materials, 1916 Race St., Philadelphia, PA, 1963, pp. 24–31.
- [28] J. Cahn, J. Hilliard, Free energy of a nonuniform system. I. Interfacial free energy, *J. Chem Phys* 28 (1958) 258.
- [29] F. Liu, H. Metiu, Dynamics of phase separation of crystal surfaces, *Physical Review B* 48 (9) (1993) 5808–5818.
- [30] A. Golovin, S. Davis, A. Nepomnyashchy, A convective Cahn-Hilliard model for the formation of facets and corners in crystal growth, *Physica D* 122 (1998) 202–230.
- [31] A. Bray, Theory of phase-ordering kinetics, *Advances in Physics* 43 (1994) 357–459.

- [32] J. Stavans, The evolution of cellular structures, *Reports on Progress in Physics* 56 (6) (1993) 733–789.
- [33] V. Fradkov, D. Udler, Two-dimensional normal grain growth: Topological aspects, *Advances in Physics* 43 (6) (1994) 739–789.
- [34] H. Frost, C. Thompson, Computer simulation of grain growth, *Current Opinion in Solid State and Materials Science* 1 (3) (1996) 361–368.
- [35] C. Thompson, Grain growth and evolution of other cellular structures, *Solid State Physics* 55 (2001) 269–314.
- [36] G. Schliecker, Structure and dynamics of cellular systems, *Advances in Physics* 51 (5) (2002) 1319–1378.
- [37] T. Schulze, R. Kohn, A geometric model for coarsening during spiral-mode growth of thin films, *Physica D* 132 (1999) 520–542.
- [38] C. Beenakker, Evolution of two-dimensional soap-film networks, *Physical Review Letters* 57 (19) (1986) 2454–2457.
- [39] H. Flyvbjerg, Model for coarsening froths and foams, *Physical Review E* 47 (6) (1993) 4037–4054.
- [40] M. Marder, Correlations and ostwald ripening, *Physical Review A* 36 (2) (1987) 858–874.